arXiv:2404.04698v1 [cs.RO] 6 Apr 2024

EAGLE: The First Event Camera Dataset Gathered by an Agile Quadruped Robot

Shifan Zhu, Zixun Xiong, and Donghyun Kim

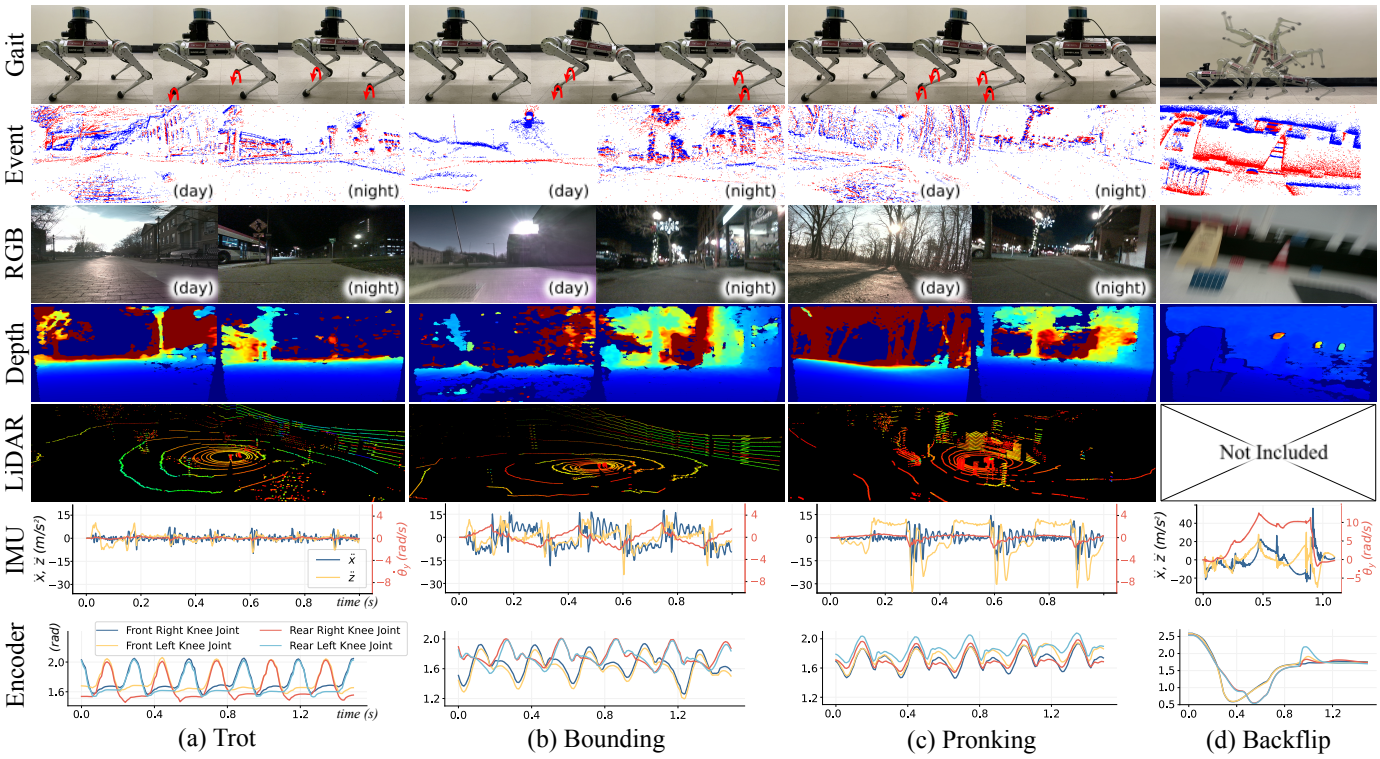

(a) Trot (b) Bounding (c) Pronking (d) Backflip

Fig. 1: **An overview of the dataset under various gaits.** The top row illustrates three different gaits and a backflip motion. The subsequent rows show different sensor data corresponding to each gait. Note that the ratios of event, RGB, and LiDAR images have been adjusted to fit into the figure.

***Abstract*—When legged robots perform agile movements, traditional RGB cameras often produce blurred images, posing a challenge for accurate state estimation. Event cameras, inspired by biological vision mechanisms, have emerged as a promising solution for capturing high-speed movements and coping with challenging lighting conditions, owing to their significant advantages, such as low latency, high temporal resolution, and a high dynamic range. However, the integration of event cameras into agile-legged robots is still largely unexplored. Notably, no event camera-based dataset has yet been specifically developed for dynamic legged robots. To bridge this gap, we introduce EAGLE (Event dataset of an AGile LEgged robot), a new dataset comprising data from an event camera, an RGB-D camera, an IMU, a LiDAR, and joint angle encoders, all mounted on a quadruped robotic platform. This dataset features more than 100 sequences from real-world environments, encompassing various indoor and outdoor environments, different lighting conditions, a range of robot gaits (e.g., trotting, bounding, pronking), as well as acrobatic movements such as backflipping. To our knowledge, this is the first event camera dataset to include multi-sensory data collected by an agile quadruped robot.**

All authors are with Manning College of Information & Computer Sciences, University of Massachusetts Amherst, MA, USA. donghyunkim@cs.umass.edu

***Index Terms*—Event camera dataset, Agile quadruped robot, Multi-sensory data.**

I. INTRODUCTION

In this paper, we introduce a comprehensive dataset tailored for quadruped robots that can perform dynamic movements in various lighting conditions and environments. The superior mobility of quadruped robots holds significant potential in applications requiring rapid navigation in complex environments including confined spaces and rough terrains. However, despite significant advancement in their locomotion capability [1], [2], their application remains limited to the scenarios without immediate needs or rapid exploration [3], [4]. This constraint delays the broader adoption of the extremely capable legged robotic system to perform hazardous and time-sensitive tasks, such as disaster response, search and rescue, and firefighting [5], [6]. One of the most pressing issues is the compromised perception capability during swift movements: motion blur in RGB images and distortion in LiDAR point clouds hinder precise pose estimation and environmental understanding.

TABLE I: Comparison of datasets with event cameras.

Dataset	Event Resolution	Depth Sensor	IMU	Platform	Environment	Ground-truth Pose
D-eDVS [7]	128×128	RGB-D	✗	Handheld	Indoor	MoCap
evbench [8]	240×180	RGB-D	✗	Wheeled robot	Indoor	Odometer
Mueggler et al. [9]	240×180	✗	✓	Handheld	Indoor/Outdoor	MoCap
MVSEC [10]	$2 \times 346 \times 260$	LiDAR-16	✓	Multiple Robots	Indoor/Outdoor	MoCap/Cartographer
UZH-FPV [11]	346×260	✗	✓	Drone	Indoor/Outdoor	MoCap
ViViD [12]	240×180	RGB-D/LiDAR-16	✓	Handheld	Indoor/Outdoor	MoCap/LeGO-LOAM
ViViD++ [13]	240×180 640×480	RGB-D/LiDAR-64	✓	Handheld/Car	Indoor/Outdoor	MoCap/LeGO-LOAM/RTK-GPS
DSEC [14]	$2 \times 640 \times 480$	LiDAR-16	✗	Car	Outdoor	RTK-GPS
AGRI-EBV [15]	240×180	RGB-D/LiDAR-16	✓	Wheeled Robot	Outdoor	LeGO-LOAM
TUM-VIE [16]	$2 \times 1280 \times 720$	✗	✓	Handheld/Bike	Indoor/Outdoor	MoCap
VECtor [17]	$2 \times 640 \times 480$	RGB-D/LiDAR-128	✓	Handheld/Scooter	Indoor	MoCap/ICP
M3ED [18]	$2 \times 1280 \times 720$	LiDAR-64	✓	Multiple Robots	Indoor/Outdoor	Faster-LIO
EAGLE	346×260 320×240	RGB-D/LiDAR-16	✓	Agile legged Robot	Indoor, Outdoor	MoCap/Faster-LIO

* Extension *-16* represents a 16-beam LiDAR.

Event cameras, similar to the human eye, detect logarithmic intensity changes in images and offer low latency and high temporal resolution, making them exceptionally suited for handling rapid robotic movements. Additionally, their high dynamic range (HDR) effectively addresses challenges in poorly-lit and brightly-lit settings, thereby broadening potential applications for robots [19], [20]. Recent studies on event cameras have increasingly gained attention in systems requiring rapid perception, such as drones and autonomous vehicles [21], [22], yet their use has not been widely recognized within the legged robot community. Once properly configured, these unique sensors can significantly enhance state estimation and terrain perception, greatly expanding the capabilities of legged robots.

While promising, event cameras also have drawbacks when used as standalone sensing systems. Due to their operating mechanism of detecting changes in brightness, event data inherently depend on the motion of the camera itself (ego-motion), making it challenging to differentiate between the camera's movement and changes in the external environment. This issue can obscure the clarity of visual data representations, especially when the robot moves slowly or in directions parallel to environmental textures. Overcoming these limitations and enhancing the functionality of agile legged robots in diverse environments necessitates the development of algorithms for the synergistic integration of multimodal sensors. However, as of 2024, there is a lack of comprehensive datasets to support this research.

To bridge this gap, we introduce a new dataset collected by a unique sensor suite on an agile quadruped robot, MIT Mini-Cheetah [23]. Our system features an event camera, an RGB-D camera, an IMU, a LiDAR, and joint angle sensors. The integration of event and RGB cameras provides the legged robot with enhanced capabilities for both slow and rapid motions. Depth information, crucial for accurate state estimation and navigation, is supplied by the RGB-D camera and LiDAR. The IMU, critical for capturing high-frequency angular and acceleration data, is inherently immune to disturbances from external dynamic objects. Furthermore, joint angle data can also provide odometry information through forward kinematics.

Our dataset includes various distinct robot gaits, including trotting, bounding, and pronking. It also encompasses a wide range of daily indoor and outdoor environments, under varying lighting conditions (e.g., daytime, nighttime, well-lit, dark, high dynamic range, and blinking light conditions). This diverse collection provides an in-depth perspective on the robot's capabilities under varying conditions and times. Throughout the dataset building, we aim to contribute to the enhancement of the legged robots' resilience and adaptability across a multitude of real-world environments.

In summary, the main contributions of this paper include:

- We present the first dataset that provides a comprehensive collection of sensor data from an agile quadruped robot, including inputs from an event camera, RGB-D camera, IMU, LiDAR, and joint encoders.
- We provide data across 31 distinct environments, within each of which we captured data under varying lighting conditions and through diverse robotic locomotion gaits.
- We offer 6 DoF ground-truth poses from a motion capture system or an advanced SLAM algorithm, complemented with precise intrinsic, extrinsic, and temporal synchronization parameters.

All the data sequences are publicly available at https://daroslab.github.io/EAGLE/.

II. RELATED WORK

The growing interest in event cameras has led to numerous datasets aimed at various research goals. In this section, we provide an overview of these event camera datasets, along with a comparative summary in Table I.

The first event camera dataset, introduced by Weikersdorfer et al. in 2014 [7], featured a 128×128 eDVS event camera [24] and an RGB-D camera. In 2016, Barranco et al. [8] utilized an event camera (240×180) for visual navigation of a mobile wheeled robot. Mueggler et al. [9], in 2017, released a comprehensive handheld dataset that includes motion speed information as a reference for investigating the capabilities of an event camera (240×180). These datasets have played a crucial role in the introduction of event cameras in research communities, yet the resolution of the event cameras used in these early stages was relatively low.

Subsequent developments have led to datasets with higher-resolution event cameras. In 2022, Lee et al. expanded the

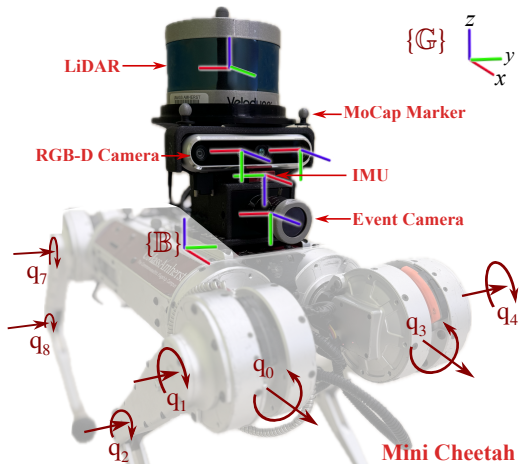

Fig. 2: **Configuration of the sensors.** All sensors are rigidly mounted on top of the Mini Cheetah robot. The coordinate systems for the sensors, the robot's body, and the global frame are indicated by the red, green, and blue axes, representing the x, y, and z directions, respectively.

ViViD dataset [12] into ViViD++ [13], incorporating a high-resolution event camera (640×480) for driving scenarios. This update included repeated data collection along the predefined trjectories at different times, categorizing motions as slow, unstable, or aggressive. Klenk et al. [16] introduced the TUM-VIE dataset with stereo event camera recordings (1280×720), capturing diverse environments and activities such as walking, running, skating, and biking. Additionally, Gao et al. [17] released the VECtor dataset, which includes head-mounted and pole-mounted stereo event camera sequences (640×480) in indoor settings. These enhanced-resolution event camera datasets improved image clarity and details, enabling more precise analysis.

In the evolution of event camera datasets, datasets for specific research purposes have also been developed. The DDD17 [25] and DDD20 [26] datasets, for instance, provide comprehensive metadata including vehicle speed, GPS positioning, and detailed driving dynamics such as steering, throttle, and brake inputs, improving steering prediction accuracy. Fischer et al. [27] aimed to tackle the place recognition challenge by mounting a DAVIS346 event camera (346×260) on a car, capturing data along the same trajectory at different times. Zujevs et al. [15] created agricultural robotics datasets in varied agricultural settings using a mobile wheeled robot. Additionally, Gehrig et al. [14] utilized a dual stereo camera setup with a 16-channel Velodyne LiDAR and an RTK-GPS system for automotive driving scenarios. These datasets delve deeper into specific fields and provide the opportunity to explore the potential of event cameras in focused applications.

Another trend in the development of event camera datasets is their application in various robotic platforms. Delmerico et al. [11] introduced a dataset focused on aggressive drone racing motions. Zhu et al. [10] launched the first multi-robot dataset in 2018, featuring indoor and outdoor places with handheld devices, hexacopters, vehicles, and motorcycles. Additionally, Chaney et al. [18] unveiled the M3ED dataset, showcasing event cameras across diverse sensor arrays on multiple robotic platforms, including unmanned aerial vehicles, wheeled ground vehicles, and legged robots. These datasets further explore the unique capabilities of event cameras across different robotic platforms.

Although the M3ED dataset explores event cameras with a quadruped robot Spot, it does not fully investigate the dynamic capabilities unique to quadruped robots, such as various gaits like trotting, pronking, and bounding. The M3ED dataset utilizes the trotting gait only within relatively slow and conservative operating regions without involving dynamic movements. In addition, the M3ED dataset only contains sparse depth images generated from point cloud maps. On the other hand, our dataset includes dense depth data, various quadruped robot gait motions, and navigation in various environments under different lighting conditions.

TABLE II: Hardware specifications

Sensor Type	Frequency	Specification
DAVIS346	N/A	Resolution: 346×260 FoV: $70^\circ \times 56^\circ$
DVXplorer Lite	N/A	320×240 FoV: $61^\circ \times 52^\circ$
RealSense D455	60	Resolution: 640×480 RGB FoV: $80^\circ \times 65^\circ$ Depth FoV: $80^\circ \times 64^\circ$
Velodyne VLP-16	10	Range: 100 meters 16 channels
VectorNav VN-100	400	3-axis accelerometer 3-axis gyroscope 3-axis magnetometer 3 DoF orientation
Mini Cheetah Motors	100	12 encoders
OptiTrack	120	8 *PrimeX-22* cameras

III. Hardware Setup

Fig. 2 illustrates our hardware setup, including an event camera, a RealSense D455 RGB-D camera, a 9-axis VectorNav IMU, a 16-channel Velodyne LiDAR, and 12 joint encoders on the Mini Cheetah robot. We use two different event cameras: a DAVIS346 event camera for outdoor and a DVXplorer Lite event camera for indoor/backflip data collection due to its superior throughput of 100 million events per second (MEPS), compared to the DAVIS346's 12 MEPS. All vision sensors and an IMU are rigidly mounted on the Mini Cheetah robot using custom 3D-printed fixtures. The Mini Cheetah's 12 actuators control its limbs, with joint numbering starting from the front right abduction/adduction joint and continuing through the hip and knee flexion/extension joints, and then extending to the front left, hind right, and hind left limbs as depicted in Fig. 2. Sensor specifications are summarized in Table II.

A. Sensors Overview

The DAVIS346 event camera (346×260 resolution), with a 70° horizontal and 56° vertical field of view and a 120 dB dynamic range, includes a built-in 6-axis IMU and the capability to capture RGB images. The DVXplorer Lite (320×240 resolution), featuring a 61° horizontal and 52° vertical field

of view and a 110 dB dynamic range, also includes a built-in 6-axis IMU but cannot output RGB images. Both cameras feature sub-millisecond latency. We put an infrared filter in front of both event cameras to block emissions from the RealSense RGB-D camera.

The RealSense camera D455 operates at 640×480 resolution and 60 Hz, with $80^\circ \times 65^\circ$ and $80^\circ \times 64^\circ$ fields of view for its RGB and depth cameras, respectively. Timestamps are set at the midpoint of exposure, and auto exposure is enabled to obtain well-exposed images in different lighting conditions. Thus, the timestamp gap between RGB and depth frames varies, typically from 0 to 8.33 ms. VectorNav VN-100 is a 9-axis IMU that comprises a 3-axis gyroscope, 3-axis accelerometer, and 3-axis magnetometer at 400 Hz. Additionally, the dataset also includes the orientation data produced by the IMU sensor in quaternion representation. The Velodyne VLP-16 LiDAR delivers highly accurate depth measurements as point clouds at 10 Hz. The LiDAR is mounted atop the Mini Cheetah, ensuring an unobstructed view of the surrounding environment. The Mini Cheetah's 12 custom motors feature joint encoders that measure angular position at 1 kHz. For this dataset, data is recorded at 100 Hz.

To gather ground-truth pose data, we use the OptiTrack motion capture (MoCap) system, equipped with 8 *PrimeX-22* cameras in a $7.5\ \mathrm{m} \times 5.5\ \mathrm{m} \times 2.8\ \mathrm{m}$ space. This setup is ideal for precise motion tracking and generating accurate 6 DoF ground-truth poses.

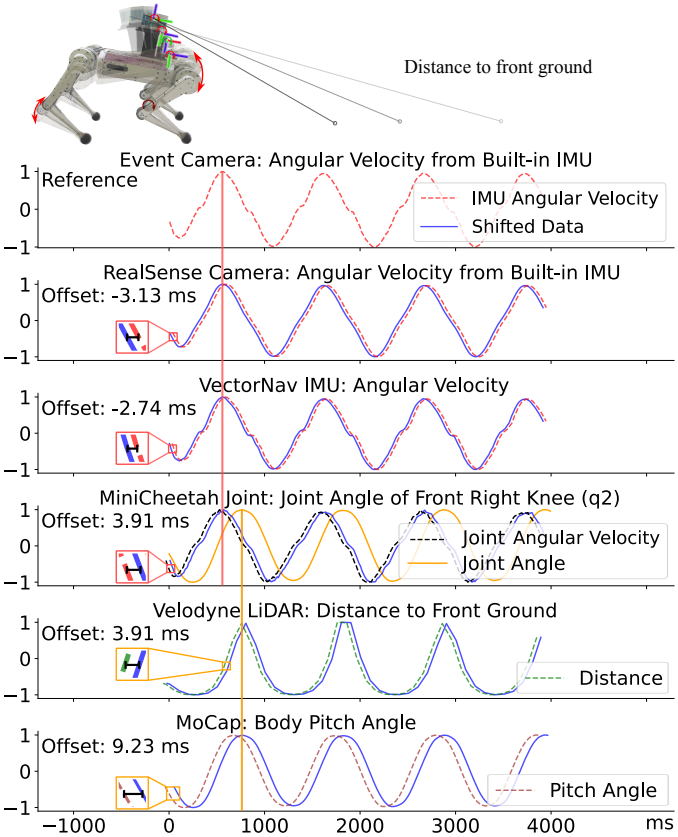

Fig. 3: **Time synchronization across different sensors.** The red vertical line indicates alignment with the RealSense camera and VectorNav IMU, using the event camera's angular velocity as a reference, while the orange line shows alignment with the Velodyne LiDAR and MoCap, referencing Mini Cheetah's joint angle. For clearer visualization, we magnified the average offset by 10 to visualize the difference of the original and synchronized data.

B. Calibration

The calibration process encompasses intrinsic calibration of cameras and an IMU, as well as extrinsic calibration across all sensors. All parameters are available on the dataset website.

1) Intrinsic Calibration: We performed intrinsic parameter calibration of event cameras to empirically measure focal length, optical center, and distortion coefficients. The Kalibr toolbox [28] is used with the grayscale images constructed from the event stream. We followed standard steps by observing a checkerboard of known dimensions from varying angles. For IMU intrinsic calibration, we used Allan Variance ROS toolbox[1], involving 6 hours of static data collection for analysis, to identify random walk and noise density of a VectorNav IMU. For the RealSense camera, we did not perform additional intrinsic parameter calibration and used onboard parameters provided by the manufacturer. For confirmation, we qualitatively validated the parameters by checking the alignment between RGB images and the depth images projected into the RGB frame.

2) Extrinsic Calibration: Extrinsic calibration process determines the spatial transformation between each pair of sensors. Due to its high image quality, we used the RealSense RGB camera as a reference to identify extrinsic parameters with other frames – an event camera, a VectorNav IMU, a LiDAR, and a robot. The Kalibr toolbox was utilized to acquire extrinsic parameters between the RealSense camera, event camera, and the VectorNav IMU, while the Autoware toolkit[2] facilitated the extrinsic calibration between the RealSense RGB camera and LiDAR. Extrinsic parameters between the RealSense RGB camera and the robot were determined from the CAD file. For the RealSense RGB and depth cameras, we used onboard extrinsic parameters provided by the manufacturer. We then derived the extrinsic parameters for all sensor pairs using the identified parameters, creating completed spatial relationships within our sensor array.

C. Time Synchronization

Although every sensor includes accurate internal clock signals, the timestamp of each clock has different offsets. Setting a single timestamp across different sensors is crucial, and hardware synchronization – a single clock source shared by multiple sensors – is often used. However, considering the outdoor data gathering, acrobatic backflip, and various sensors (e.g., motion capture and the robot's joint encoders), the hardware connection of all sensors was not a practical option

[1]https://github.com/ori-drs/allan_variance_ros

[2]https://github.com/autowarefoundation/autoware

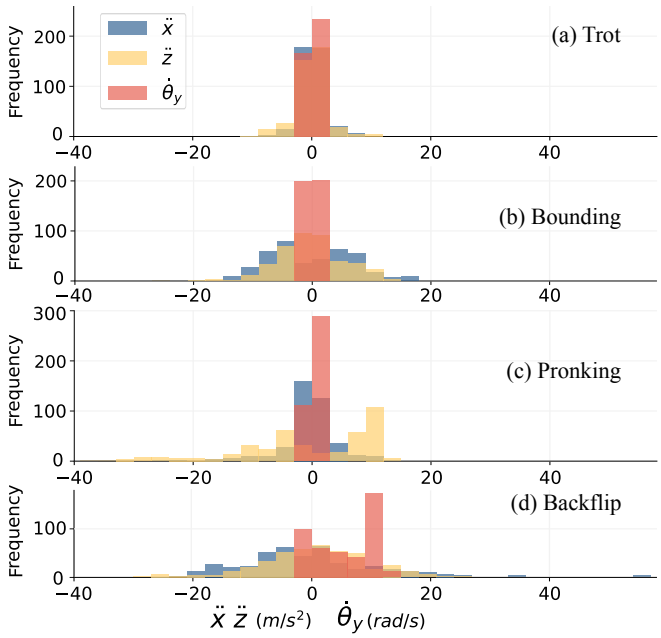

Fig. 4: **Histograms of forward/vertical accelerations, and pitch angular velocity during different gaits.** The histogram depicts the unique features of each gait. Compared to the stable trot gait, the pronking gait exhibits high-dynamic vertical movement, as indicated by high $\ddot{z}$ values. Similarly, the backflip motion shows distinctive high body pitch velocity ($\dot{\theta}_y$) and a wide range of acceleration ($\ddot{x}$, $\ddot{z}$).

for us. Instead, we introduced a specific motion designed for accurate temporal synchronization through post-processing.

Every time we start the data collection, the Mini-cheetah performs a body pitching swing to produce specific sinusoidal patterns in the sensor data. Since each camera sensor includes built-in IMU sensors, we compare the angular velocity data from the IMUs in the event and RealSense cameras with that of the VectorNav IMU. During this process, an event camera is used as a reference, and the timestamps of other sensors are offset based on it. Then, the robot's joint encoder data are synchronized with the event cameras by comparing the angular velocities of the knee joint and the built-in IMU of the event camera.

For the LiDAR and MoCap data synchronization, we used joint position data as a reference. Synchronizing the LiDAR sensor is particularly challenging due to the lack of a velocity measurement sensor such as an IMU. To make a sinusoidal pattern in LiDAR data, we perform the pitch swing sequence on flat ground and use the distance from the LiDAR sensor to the front ground as a pattern for matching. By comparing this distance, the robot's knee joint angles, and the body pitch computed from MoCap data, we performed temporal synchronization across all sensors.

In the computation of temporal offset between sensors, we initially normalized all data to standardize measurement scales. We then uniformly sampled 10000 data points from all sensor data by applying linear interpolation to account for the different sampling rates of each sensor. Using these sampled data, we calculated temporal offsets by maximizing cross-correlation. Note that each data sequence includes a body pitch swing motion as well as a ball thrown in front of the robot. This ball data was used to verify the temporal synchronization accuracy across all camera sensors. Fig. 3 illustrates the time synchronization results.

IV. Dataset

The EAGLE dataset contains 106 sequences including 50 indoor, 40 outdoor, and 16 backflip sequences. Our dataset aims to evaluate algorithm performance: 1) across diverse quadruped gaits and lighting conditions via indoor and outdoor sequences, and 2) in highly dynamic motions through backflip sequences. The name of each sequence reflects the recording environment, lighting conditions, and the gaits of the quadruped robot. For instance, *downtown1_day_trot* represents data gathered in a downtown environment during daytime with a trot gait, while *classroom_blinking_comb* indicates data collected in a classroom environment under blinking light conditions with a combination of trotting, bounding, and pronking gaits. Fig. 4 further illustrates dynamic characteristics inherent to each gait. In addition, we marked the initial positions of the robot's four feet in each sequence and confirmed its return to these exact positions, providing an additional metric for pose estimation.

A. Outdoor Sequences

The outdoor sequences were captured in 10 distinctive outdoor environments, with four sequences per environment. Each set of four sequences includes variations of two different sets of quadruped gaits (trot-only and combined gaits) under different periods of the day (daytime and nighttime), ensuring a comprehensive representation of real-world settings. Fig. 5 provides an illustration of all outdoor environments and associated challenges such as varied light conditions from overexposure to underexposure, sunny, cloudy, and foggy weather, diverse visual patterns including featureless terrains and distant skies, dynamic objects (e.g., vehicles and pedestrians), and slippery surfaces. The inclusion of these elements in our dataset mirrors a wide range of real-world challenges, broadening the evaluation spectrum and offering a comprehensive assessment opportunity.

B. Indoor Sequences

The indoor sequences were collected in 13 diverse environments. In the dining hall, building floor, and home environments, we recorded two sequences per site, with each sequence showcasing a different set of quadruped gaits. For other indoor environments where we can control the lighting condition, data collection was expanded to encompass a range of lighting conditions – well-lit, dark, HDR, and blinking – while consistently applying two sets of quadruped gaits within each lighting condition. Specifically, in laboratory environments, four sequences were recorded in one site under both consistently well-lit and HDR lighting conditions. To make HDR condition, we used bright light sources in a dark environment. In classroom and kitchen environments, we gathered six sequences in each place across well-lit, HDR, and

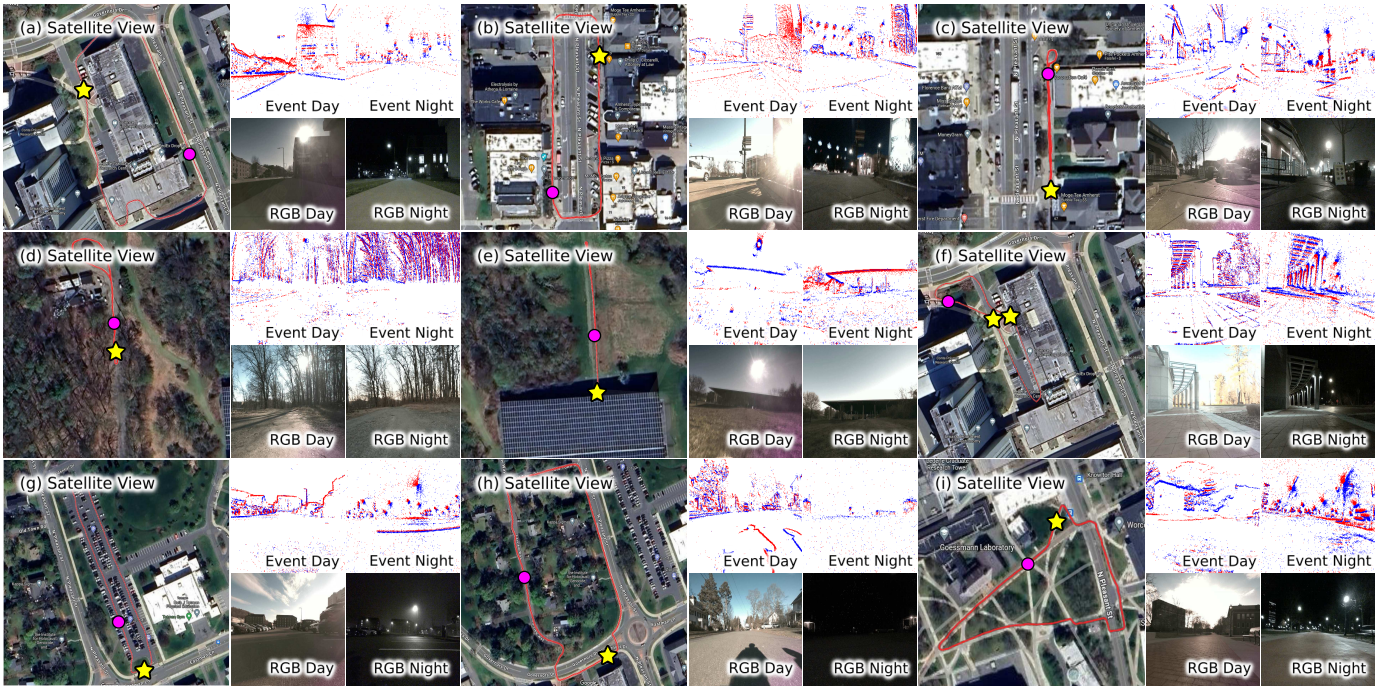

Fig. 5: **Overview of 10 outdoor environments.** (a) is the area around a campus building with a direct sunlight source. (b) and (c) are downtown areas containing dynamic elements like pedestrians, vehicles, and blinking lights. (d) is a forest environment that includes slippery ground. (e) is a grassy environment with featureless ground, expansive space, and distant sky. (f) includes a short sidewalk path and a route between two buildings, highlighting a standard pedestrian space environment. (g) is a parking lot during a cloudy day and a foggy night. (h) is a residential area with complete darkness at night. (i) presents a long sidewalk path, illustrating several pavement types. Event and RGB images are presented with satellite views at each site, showing day and night scenes at the same location, indicated by purple circles. The yellow star marks the start/end points, and the red path denotes the trajectory.

blinking lighting conditions. In the MoCap space, we arranged various objects on the ground to create three different scenes, recording six sequences in each environment under well-lit, dark, and blinking lighting conditions.

Indoor sequences, similar to outdoor ones, also encounter challenges such as diverse lighting conditions, dynamic objects, and slippery floors. Additionally, indoor sequences introduce unique challenges: light reflections from surfaces such as floors and glasses can complicate perception, and closely positioned obstacles may briefly obstruct cameras' view, adding extra complexity to navigation and sensing.

C. Backflip Sequences

The backflip, demonstrating the robot's dynamic capabilities with rotations up to $750°/\mathrm{s}$, was captured in 7 indoor environments and 1 outdoor environment, with two sequences in each environment. We excluded the LiDAR sensor due to its substantial weight, which can bother the success of the acrobatic movement, and the significant motion distortion in the point cloud data. Each sequence contains three consecutive backflips, after which the robot returns to the initial marked position.

Backflip sequences present distinct challenges that are different from indoor and outdoor sequences. The backflip motion's high speed lead to significantly blurred images from the RealSense RGB camera. Ground contact causes abrupt changes in acceleration and angular velocity (Fig. 1 and Fig. 4), posing significant challenges for visual-inertial systems and serving as a crucial test for their adaptability in highly dynamic robot motions. Another unique challenge in backflip sequence is the difficulty in feature detection. Although we chose environments that offer visual features from multiple angles, captured images may appear featureless when the camera's view is directed toward the bare ceiling or floor.

D. Limitations

During data gathering, we observed two artifacts that could be potential limitations of the dataset. The first is occasional missing event data in outdoor daytime sequences, particularly in environments with complex textures, attributed to the limited throughput of the DAVIS346 event camera (RGB + Event). The second artifact is blinking dot noise observed in the dark regions of RGB images captured by the RealSense camera. This noise becomes apparent when the camera's auto-exposure feature is enabled to optimize performance in high dynamic range environments.

V. Evaluation

To assess the difficulty of the dataset and the quality of the parameters, we tested various sequences with state-of-

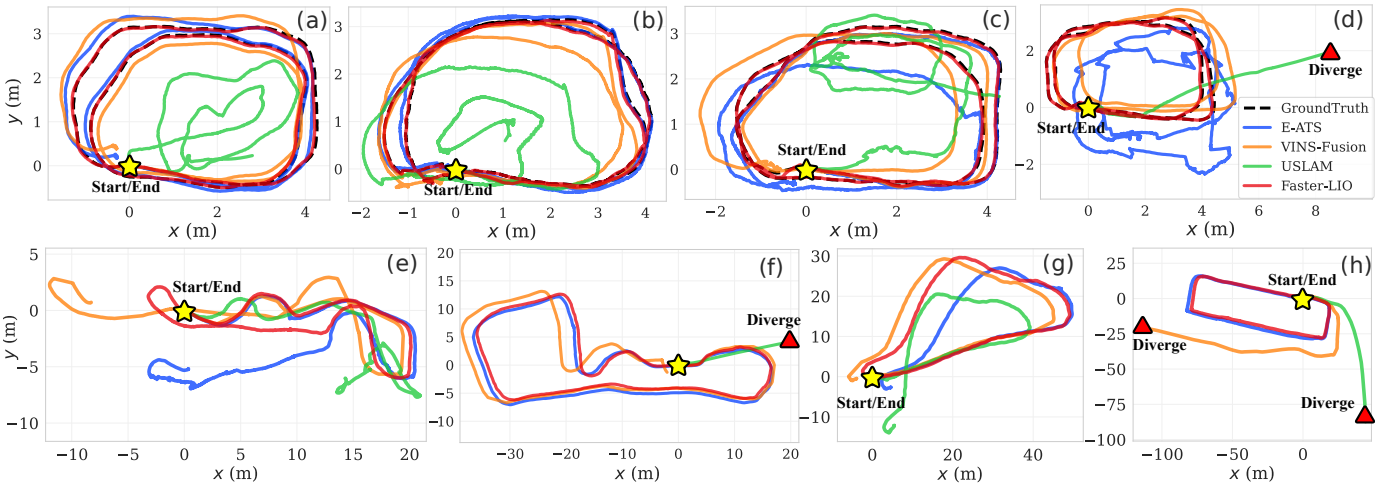

Fig. 6: **Results of various SLAM algorithms on our dataset.** (a), (b), (c), and (d) are within an indoor MoCap environment, featuring a trot gait in a well-lit environment, mixed gaits in a well-lit environment, a trot gait in a dark environment, and a trot gait under blinking lighting condition, respectively. (e) is a lab environment with mixed gaits under an HDR lighting condition. (f) occurs in a public space with a trot gait under a well-lit lighting condition. (g) and (h) are outdoor scenarios, with (g) occurring on a sidewalk with a trot gait during the daytime, and (h) presenting a downtown street with mixed gaits during nighttime. The yellow star marks the starting/ending positions and the red triangle indicates the point of divergence.

TABLE III: Comparison on EAGLE Dataset. $[\mathbf{R}_{\text{rpe}} : {}^{\circ}/\text{s}, \mathbf{t}_{\text{rpe}} : \text{cm/s}, \mathbf{t}_{\text{ate}} : \text{cm}]$

	Faster-LIO			VINS-Fusion			USLAM			E-ATS		
	$\mathbf{R}_{\text{rpe}}$	$\mathbf{t}_{\text{rpe}}$	$\mathbf{t}_{\text{ate}}$	$\mathbf{R}_{\text{rpe}}$	$\mathbf{t}_{\text{rpe}}$	$\mathbf{t}_{\text{ate}}$	$\mathbf{R}_{\text{rpe}}$	$\mathbf{t}_{\text{rpe}}$	$\mathbf{t}_{\text{ate}}$	$\mathbf{R}_{\text{rpe}}$	$\mathbf{t}_{\text{rpe}}$	$\mathbf{t}_{\text{ate}}$
mocap_env1_trot (Fig. 6(a))	0.88	2.53	**4.43**	**0.59**	3.28	29.35	5.16	26.39	157.92	0.60	**1.15**	17.29
mocap_env1_comb (Fig. 6(b))	1.11	3.16	**10.72**	**0.60**	2.62	36.88	2.30	10.61	194.41	0.77	**1.41**	45.24
mocap_env1_dark_trot (Fig. 6(c))	**0.86**	**2.78**	**3.60**	0.98	4.62	41.30	2.86	25.19	154.57	1.34	3.50	71.84
mocap_env1_dark_comb	1.24	**3.35**	**5.91**	**0.75**	4.72	45.83	2.02	20.03	223.14	2.00	4.02	90.17
mocap_env1_blink_trot (Fig. 6(d))	**0.99**	**3.24**	**5.52**	1.13	6.60	60.20	−/−	−/−	−/−	3.00	15.54	160.88
mocap_env1_blink_comb	1.11	**3.12**	**6.36**	**1.03**	4.50	54.38	2.84	24.44	284.74	5.75	19.25	180.40
env5_backflip1 (Fig. 7)	×	×	×	−/0.98	−/0.94	−/5.60	−/2.62	−/2.14	−/2.91	−/**0.79**	−/**0.80**	−/**1.02**
lab1_hdr_comb (Fig. 6(e))	∗	∗	∗	**1.10**	10.54	329.18	−/1.19	−/20.91	−/382.30	1.42	**6.35**	**250.26**
learning_center_trot (Fig. 6(f))	∗	∗	∗	**0.75**	10.61	206.27	−/−	−/−	−/−	0.78	**5.58**	**104.09**
sidewalk1_day_trot (Fig. 6(g))	∗	∗	∗	1.12	**14.40**	196.51	1.88	39.66	1114.87	**1.00**	16.93	388.23
downtown1_night_comb (Fig. 6(h))	∗	∗	∗	−/0.91	−/78.13	−/1833	−/0.91	−/186.3	−/1694	**0.77**	**7.86**	**224.93**
residential_area_night_comb	−/−	−/−	−/−	−/−	−/−	−/−	−/−	−/−	−/−	−/−	−/−	−/−

The symbol / differentiates evaluations on partial and full trajectories, with partial ones manually truncated and evaluated before significant divergence. The symbol × means not included. RPE for backflip sequences is assessed at 0.1-second intervals.

the-art algorithms for several sensor pairs, including Faster-LIO (LiDAR + IMU) [29], E-ATS (Event + RGB-D) [30], UltimateSLAM (Event + RGB + IMU, noted as USLAM) [19], and VINS-Fusion (RGB + IMU) [31]. USLAM operates in event-IMU mode for indoor evaluations due to the lack of RGB images from the event camera, and switches to event-RGB-IMU mode for outdoor environments.

For sequences captured within the MoCap environment (labeled as *mocap_**), we use ground-truth poses from the MoCap system for evaluation. For sequences without a MoCap system, we use the pose estimated by the Faster-LIO algorithm as ground truth because the estimation results of the Faster-LIO algorithm demonstrate good matches between the initial and final poses, as shown in Fig. 6. Also, the Faster-LIO shows superior accuracy on indoor MoCap sequences as evidenced in Table III. We evaluate each algorithm based on two key metrics: Absolute Pose Error (APE) and Relative Pose Error (RPE). For RPE computation, rotation is measured in degrees per second and translation is measured in centimeters per second, except for backflip sequences where we measure in degrees and centimeters per 0.1 seconds because the duration of one backflip motion is short. APE is measured in centimeters to evaluate pose estimation accuracy. The evaluation is based on the open-source software EVO[3]. The evaluation results are summarized in Table III to provide a quantitative comparison.

Fig. 6 and Fig. 7 offer a qualitative visualization. The results show that most algorithms achieve accurate pose estimation with trot gait and a well-lit lighting condition (Fig. 6 (a)). However, pose estimation accuracy drops with more dynamic gaits such as bounding and pronking gaits (Fig. 6 (b)), and in challenging dark or blinking lighting conditions (Fig. 6 (c, d)). Notably, backflip sequences, containing three consecutive backflips, present significant challenges that lead to the divergence of all tested algorithms. Consequently, our evaluation focuses on the accuracy within a single backflip to assess algorithm performance during the extreme dynamic motion (Fig. 7). Among the three tested algorithms, only one (E-ATS) survived from divergence. Our evaluation results imply that the

[3]https://github.com/MichaelGrupp/evo

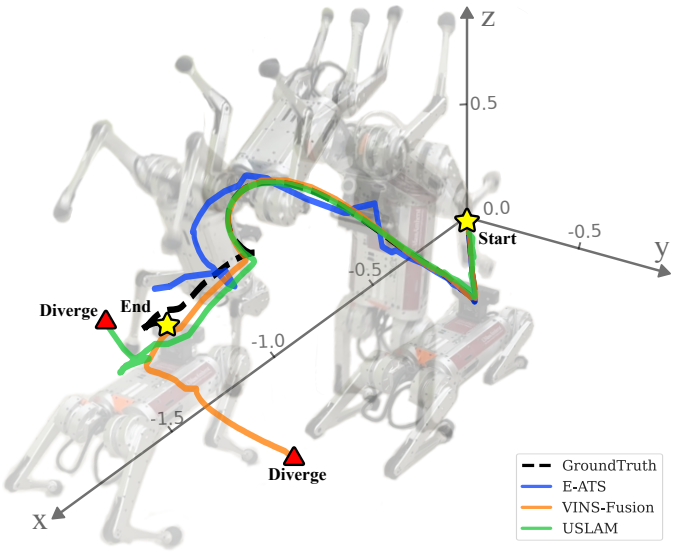

Fig. 7: **Estimated results of a backflip sequence.** This sequence is a subset of env5_backflip1 and contains one of the three backflips. The yellow star marks the starting and ending positions and the red triangle indicates the divergence.

dataset includes sufficiently challenging scenarios for state-of-the-art visual-inertial algorithms and can serve as valuable assets for future benchmarks of advanced event-based visual-inertial odometry algorithms.

VI. CONCLUSIONS

In this paper, we introduce the EAGLE dataset, the pioneering dataset designed to investigate the utilization of an event camera, RGB-D camera, LiDAR, IMU, and joint encoders on an agile quadruped robot. The EAGLE dataset offers a rich collection of indoor and outdoor sequences under various quadruped gaits and lighting conditions. Additionally, it includes backflip sequences that highlight the agility of the robot. We envision the EAGLE dataset as a cornerstone for propelling forward research in event camera applications in the field of legged robotics.

ACKNOWLEDGMENT

We express our gratitude to Naver Labs and MIT Biomimetic Robotics Lab for providing the Mini-cheetah robot as a research platform for conducting dynamic motion studies on legged robots.

REFERENCES

[1] D. Kim *et al.*, "Highly dynamic quadruped locomotion via whole-body impulse control and model predictive control," *arXiv preprint arXiv:1909.06586*, 2019.
[2] G. B. Margolis *et al.*, "Rapid locomotion via reinforcement learning," *arXiv preprint arXiv:2205.02824*, 2022.
[3] T. Rouček *et al.*, "Darpa subterranean challenge: Multi-robotic exploration of underground environments," in *Modelling and Simulation for Autonomous Systems: 6th International Conference, MESAS 2019, Palermo, Italy, October 29–31, 2019, Revised Selected Papers 6*. Springer, 2020, pp. 274–290.
[4] F. Jenelten *et al.*, "Dtc: Deep tracking control," *Science Robotics*, vol. 9, no. 86, p. eadh5401, 2024.
[5] T. Yoshiike *et al.*, "Development of experimental legged robot for inspection and disaster response in plants," in *International Conference on Intelligent Robots and Systems (IROS)*. IEEE, 2017, pp. 4869–4876.
[6] B. Lindqvist *et al.*, "Multimodality robotic systems: Integrated combined legged-aerial mobility for subterranean search-and-rescue," *Robotics and Autonomous Systems*, vol. 154, p. 104134, 2022.
[7] D. Weikersdorfer *et al.*, "Event-based 3d slam with a depth-augmented dynamic vision sensor," in *International Conference on Robotics and Automation*. IEEE, 2014, pp. 359–364.
[8] F. Barranco *et al.*, "A dataset for visual navigation with neuromorphic methods," *Frontiers in neuroscience*, vol. 10, p. 49, 2016.
[9] E. Mueggler *et al.*, "The event-camera dataset and simulator: Event-based data for pose estimation, visual odometry, and slam," *The International Journal of Robotics Research*, vol. 36, pp. 142–149, 2017.
[10] A. Z. Zhu *et al.*, "The multivehicle stereo event camera dataset: An event camera dataset for 3d perception," *Robotics and Automation Letters*, vol. 3, no. 3, pp. 2032–2039, 2018.
[11] J. Delmerico *et al.*, "Are we ready for autonomous drone racing? the uzh-fpv drone racing dataset," in *International Conference on Robotics and Automation*. IEEE, 2019, pp. 6713–6719.
[12] A. J. Lee *et al.*, "Vivid: Vision for visibility dataset," in *International Conference on Robotics and Automation Workshops*. IEEE, 2019.
[13] ——, "Vivid++: Vision for visibility dataset," *Robotics and Automation Letters*, vol. 7, no. 3, pp. 6282–6289, 2022.
[14] M. Gehrig, W. Aarents, D. Gehrig, and D. Scaramuzza, "Dsec: A stereo event camera dataset for driving scenarios," *Robotics and Automation Letters*, vol. 6, no. 3, pp. 4947–4954, 2021.
[15] A. Zujevs *et al.*, "An event-based vision dataset for visual navigation tasks in agricultural environments," in *International Conference on Robotics and Automation (ICRA)*. IEEE, 2021, pp. 13 769–13 775.
[16] S. Klenk *et al.*, "Tum-vie: The tum stereo visual-inertial event dataset," in *International Conference on Intelligent Robots and Systems (IROS)*. IEEE, 2021, pp. 8601–8608.
[17] L. Gao *et al.*, "Vector: A versatile event-centric benchmark for multi-sensor slam," *Robotics and Automation Letters*, vol. 7, no. 3, pp. 8217–8224, 2022.
[18] K. Chaney *et al.*, "M3ed: Multi-robot, multi-sensor, multi-environment event dataset," in *Proceedings of the IEEE/CVF Conference on Computer Vision and Pattern Recognition*, 2023, pp. 4015–4022.
[19] A. R. Vidal *et al.*, "Ultimate slam? combining events, images, and imu for robust visual slam in hdr and high-speed scenarios," *Robotics and Automation Letters*, vol. 3, no. 2, pp. 994–1001, 2018.
[20] H. Rebecq *et al.*, "High speed and high dynamic range video with an event camera," *IEEE transactions on pattern analysis and machine intelligence*, vol. 43, no. 6, pp. 1964–1980, 2019.
[21] D. Falanga *et al.*, "Dynamic obstacle avoidance for quadrotors with event cameras," *Science Robotics*, vol. 5, no. 40, p. eaaz9712, 2020.
[22] G. Chen *et al.*, "Event-based neuromorphic vision for autonomous driving: A paradigm shift for bio-inspired visual sensing and perception," *Signal Processing Magazine*, vol. 37, no. 4, pp. 34–49, 2020.
[23] B. Katz *et al.*, "Mini cheetah: A platform for pushing the limits of dynamic quadruped control," in *2019 international conference on robotics and automation (ICRA)*. IEEE, 2019, pp. 6295–6301.
[24] J. Conradt *et al.*, "An embedded aer dynamic vision sensor for low-latency pole balancing," in *International Conference on Computer Vision Workshops*. IEEE, 2009, pp. 780–785.
[25] J. Binas *et al.*, "Ddd17: End-to-end davis driving dataset," *arXiv preprint arXiv:1711.01458*, 2017.
[26] Y. Hu *et al.*, "Ddd20 end-to-end event camera driving dataset: Fusing frames and events with deep learning for improved steering prediction," in *International Conference on Intelligent Transportation Systems*. IEEE, 2020, pp. 1–6.
[27] T. Fischer *et al.*, "Event-based visual place recognition with ensembles of temporal windows," *Robotics and Automation Letters*, vol. 5, no. 4, pp. 6924–6931, 2020.
[28] P. Furgale *et al.*, "Unified temporal and spatial calibration for multi-sensor systems," in *International Conference on Intelligent Robots and Systems*. IEEE, 2013, pp. 1280–1286.
[29] C. Bai *et al.*, "Faster-lio: Lightweight tightly coupled lidar-inertial odometry using parallel sparse incremental voxels," *Robotics and Automation Letters*, vol. 7, no. 2, pp. 4861–4868, 2022.
[30] S. Zhu *et al.*, "Event camera-based visual odometry for dynamic motion tracking of a legged robot using adaptive time surface," in *International Conference on Intelligent Robots and Systems*. IEEE, 2023.
[31] T. Qin *et al.*, "A general optimization-based framework for local odometry estimation with multiple sensors," 2019.